



# Preparation and performance of polymer electrolyte based on poly(vinylidene fluoride)/polysulfone blend membrane via thermally induced phase separation process for lithium ion battery

Qiao Cheng <sup>a</sup>, Zhenyu Cui <sup>a,\*</sup>, Jiangbo Li <sup>a</sup>, Shuhao Qin <sup>b</sup>, Feng Yan <sup>a</sup>, Jianxin Li <sup>a</sup>

<sup>a</sup> State Key Laboratory of Hollow Fiber Membrane Materials and Processes, School of Materials Science and Engineering, Tianjin Polytechnic University, Tianjin 300387, PR China

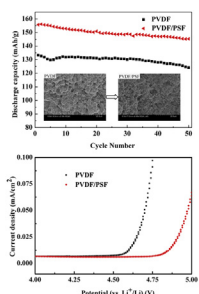
<sup>b</sup> National Engineering Research Center for Compounding and Modification of Polymer Materials, Guiyang 550014, PR China



## HIGHLIGHTS

- Polymer electrolyte based on PVDF/PSF blend membrane was prepared via TIPS process.
- Blending PSF promoted the nucleation of PVDF, decreased the size of PVDF spherulite.
- Blending PSF increased the electrochemical stability window of polymer electrolytes.
- Blending PSF markedly enhanced large current charge/discharge performance of cells.

## GRAPHICAL ABSTRACT



## ARTICLE INFO

### Article history:

Received 13 February 2014

Received in revised form

10 May 2014

Accepted 12 May 2014

Available online 21 May 2014

### Keywords:

Poly(vinylidene fluoride)/polysulfone blend membrane

Thermally induced phase separation

Polymer electrolyte

Lithium ion battery

## ABSTRACT

Poly(vinylidene fluoride)/polysulfone (PVDF/PSF) blend microporous matrix of polymer electrolyte for lithium ion battery is prepared via thermally induced phase separation (TIPS) technique. Because of only one parameter, i.e., the PSF/PVDF weight ratio, the membrane microstructure is conveniently controlled. The membrane formation mechanism of PVDF/PSF blend membranes is proposed with the assistance of a binary PSF/PVDF weight ratio-temperature phase diagram. In addition to studying the microstructure and mechanical properties of PVDF/PSF blend membrane, the relationship between properties of membrane, electrochemical performances of corresponding polymer electrolyte and membrane microstructure are also discussed in this paper. It is found that the addition of PSF not only increases ionic conductivity and electrochemical stable window of polymer electrolyte, but also markedly enhances charge–discharge performances of coin cell. The results reveal that PVDF/PSF blend microporous membranes prepared via TIPS technique can be used as polymer matrices of polymer electrolytes for lithium ion batteries.

© 2014 Elsevier B.V. All rights reserved.

## 1. Introduction

Lithium ion batteries have been widely applied in portable electronics, electrical vehicles, large power sources and energy storage equipments due to the high specific energy, high efficiency and long cycle life. However, scaling up the lithium battery technology for these applications is still problematic since safety issue

\* Corresponding author.

E-mail address: [cuiheyhh@163.com](mailto:cuiheyhh@163.com) (Z. Cui).

is still to be solved [1]. The safety issue of a lithium ion battery is mainly caused by the usage of liquid organic solvents in the electrolyte. Alternatively, polymer electrolyte provides an ideal way to solve the safety issue due to its adaptation to various geometries and safety [2]. Generally, two methods are employed to prepare polymer electrolytes. The most common approach is solvent casting [3,4]. According to this method, a mixture of polymer, a lithium salt, and a plasticizer is formed in a glove box and cast to form a gel polymer electrolyte (GPE). However, the mechanical strength of GPEs is poor because they were softened by the addition of liquid electrolyte. Chemical cross-linking based on polyolefin separators is a useful way to enhance mechanical properties and dimensional stability. For example, Q. Lu et al. [5] prepared hydrophilic polytetrafluoroethylene (PTFE)-supported GPE based on the cross-linked poly (ethylene glycol) and poly (glycidyl methacrylate) block copolymer (PEG-b-PGMA). The poly (ethylene glycol) side chains of PEG-b-PGMA can hold the liquid electrolyte inside GPE and PTFE offers mechanical support. The results showed that GPE not only exhibits good electrochemical performances, but also demonstrates non-flammability and good dimensional stability at elevated temperature. The phase inversion technique, suggested by Gozdz and coworkers [6], is another popular method to prepare polymer electrolyte [7,8]. This method involves an activation process in which a membrane is soaked in an electrolyte solution to form polymer electrolyte. Compared with the solvent casting technique, this technique requires critical moisture control only during the assembling process. In the activation process of the phase inversion technique, the liquid electrolyte immerses in the pores and swells the amorphous phase of the membrane. The research of Saito et al. [9] suggests that both pore structure and amorphous domain of microporous membrane influence the ionic conductivity and electrolyte reservation of corresponding polymer electrolyte. Therefore, the performance of polymer electrolyte can be improved by controlling the pore structure and the ratio of amorphous domain of microporous membrane.

In the phase inverse technique, microporous membranes have been extensively prepared by Bellcore's technology or non-solvent induced phase separation (NIPS) technique. Recently, a few studies have been reported on the preparation of microporous membranes via thermally induced phase separation (TIPS) technique. The TIPS process begins by dissolving a polymer in a diluent at a higher temperature. The solution is then cast or extruded into the desired shape (flat sheet, hollow fiber, etc.) and cooled to induce phase separation and polymer solidification (crystallization or glass transition). The diluent is extracted by solvent exchange to yield a microporous structure. When thermal energy is removed, the homogeneous polymer/diluent system can occur via solid–liquid (S–L) or liquid–liquid (L–L) phase separation depending on the polymer–diluent interaction, the composition and the thermal driving force [10]. In comparison to other membrane preparation techniques, TIPS technique is more reliable for controlling the membrane structure because the factors of influencing membrane structure are fewer. Moreover, the membranes prepared via TIPS technique show higher porosity and excellent mechanical strength [11–15].

Semi-crystalline PVDF shows some prominent advantages, such as good electrochemical stability and good affinity with liquid electrolyte. Therefore, PVDF is considered as the next generation polymer matrix candidate for higher performance lithium ion batteries [16,17]. The research of Ji et al. [11] showed that TIPS technique was an effective method to prepare PVDF matrix, and ionic conductivity of corresponding polymer electrolyte was more than  $1.0 \times 10^{-3} \text{ S cm}^{-1}$  at 25 °C. The value reached the standard of practical application for lithium ion batteries [18].

Blending is a simple and effective method to improve the performance of microporous membranes. When a blend is added to a polymer/diluent system, the interaction between polymer and diluent is changed and the crystallization process of crystalline polymer is influenced. That is, blending changes the thermodynamics and kinetic of phase separation process for a polymer/diluent system [11,19–21]. Therefore, the pore structure can be controlled. Several blend membranes, such as poly (vinyl butyral) (PVB)/pluronic F127 (F127) [19], poly(ethylene-co-vinylalcohol) (EVOH)/poly(vinylpyrrolidone) (PVP) [20] and high density polyethylene/poly(ethylene-block-ethylene glycol) (HDPE/PE-b-PEG) [21], had been prepared via TIPS technique and investigated. In recent years, some studies on PVDF blend matrix for polymer electrolyte have been carried out. For example, Cui et al. [22] prepared PVDF/polyethylene oxide-co-polypropylene oxide-co-polyethylene oxide (PEO-PPO-PEO) blend matrix and the ionic conductivity of corresponding polymer electrolyte was more than  $1.0 \times 10^{-3} \text{ S cm}^{-1}$  at 20 °C. Ma et al. [23] prepared PVDF/poly(-methyl methacrylate) (PMMA) blend matrix. It was found that PMMA reduced electrolyte leakage significantly. These investigations indicated that the PVDF blend membrane prepared via TIPS technique can be used as the polymer microporous matrix of polymer electrolyte for lithium ion batteries.

Nevertheless, there still exist some problems for the two systems in Refs [22,23]. For example, during the cooling process, the PVDF/PEO-PPO-PEO/diluent system underwent S–L phase separation and large spherulite structure was formed. The addition of PEO-PPO-PEO could not decrease spherulite size. It is clear that larger spherulite size decreases the mechanical properties of membrane and leads to the wider pore size distribution. Moreover, the electrochemical stability window of the two polymer electrolytes decreases with the addition of blend polymer. To overcome these disadvantages, PSF is selected to blend with PVDF in this study. On one hand, PSF is only partially compatible with PVDF [24–26]. Therefore the addition of PSF can weaken the interaction between PVDF and diluent. i.e., PSF can influence the membrane formation mechanism and control membrane structure. On the other, the rigid segments of benzene ring in PSF molecules have the ability to promote the nucleation for PVDF crystallization and thus decrease the spherulite size of PVDF. Finally, PSF is a kind of amorphous polymer and has a good affinity with liquid electrolyte. This suggests that blending PSF may increase the performance of the polymer electrolytes.

In this study, firstly, PVDF/PSF blend membranes were prepared by TIPS technique. Then, the membranes were soaked in liquid electrolyte and activated to form polymer electrolytes. The aim of the present study was to demonstrate the effect of PSF on the membrane formation mechanism of PVDF/diluent system and control the membrane structure systematically by varying PSF/PVDF weight ratio. The relationship between performances of membrane, electrochemical properties of corresponding polymer electrolyte and final membrane microstructure were also discussed in this paper.

## 2. Experimental

### 2.1. Materials

PVDF (Solef 1015, Mn =  $3.37 \times 10^5$ , Mw =  $5.73 \times 10^5$ ) was purchased from Solvay Silexis, Belgium. PSF ( $\eta$  = 0.62) was purchased from Dalian polysulfone Plastic Co. Ltd., P. R. China. PVDF and PSF were dried in a vacuum oven at 50 °C for 48 h before use. The mixture, composed of diethylene glycol dibenzoate (DEDB, provided by Shanghai Chemical Reagent Co., Ltd.) and dibutyl phthalate (DBP, provided by Tianjin Guangfu Fine Chemical

Research Institute, P. R. China), was used as diluent. Ethanol was used as the extractant. The liquid electrolyte, which was provided by Zhangjiagang Guotai-huarong New Materials Co. Ltd., P. R. China, was made by dissolving 1 mol L<sup>-1</sup> LiPF<sub>6</sub> in dimethyl carbonate/ethyl methyl carbonate/ethylene carbonate (1/1/1 by weight) solution. LiFePO<sub>4</sub> power, lithium tablet, acetylene black, PVDF binder and N-methyl-2-pyrrolidone (NMP) were purchased from DLG battery Co. Ltd., P. R. China.

## 2.2. Preparation of PVDF/PSF blend samples

Homogeneous PVDF/PSF/diluent solidified samples were prepared as described in previous investigation [11]. The weight ratio of PVDF/DEDB/DBP was kept at 20/20/60. The weight ratios of PSF/PVDF were 0/100, 2/100, 4/100, 6/100, 8/100 and 10/100. PVDF was dissolved in diluents and stirred at 170 °C to form homogeneous solution. Then, PSF was added to the solution under vigorous stirring for 2 h at 200 °C to get the PVDF/PSF/diluent solution. The resulting solution was quenched in liquid nitrogen to solidify.

## 2.3. Determination of the phase diagram

The cloud point ( $T_{\text{cloud}}$ ) and the dynamic crystallization temperature ( $T_c$ , i.e., the temperature that the polymer/diluent system began to crystallize) of PVDF/PSF/diluent system were measured according to the Ref. [11]. Homogeneous PVDF/PSF/diluent solidified sample was prepared as described in Section 2.2. The solidified sample was placed between a pair of microscope cover slips. Then, the solidified sample was heated up on a hot stage (Linkam THMS600) to 200 °C and cooled down to 40 °C at a controlled cooling rate of 10 °C min<sup>-1</sup>.  $T_{\text{cloud}}$  was determined visually by observing the appearance of liquid droplets under an optical microscope (Nikon Eclipse E600 POL).  $T_c$  was determined by DSC (Perkin–Elmer DSC-7). About 10 mg of the solidified sample was sealed in an aluminum DSC pan, melted at 200 °C for 3 min to erase thermal history and cooled to 40 °C at 10 °C min<sup>-1</sup>. The onset temperature of the exothermic peak during the cooling process was taken as  $T_c$ .

## 2.4. Preparation of microporous PVDF/PSF blend membranes

Homogeneous PVDF/PSF/diluent solidified samples were prepared as described in section 2.2. Then, the solidified sample was chopped into small pieces and compressed in a mold at 200 °C to form a thin film. After the mold was quenched in an ice water bath, the diluent was extracted with ethanol for 24 h. The final microporous blend membranes were vacuum freeze-dried for 12 h. The code and composition of the blend membranes and corresponding polymer electrolytes were listed in Table 1.

## 2.5. Membrane characterization

The membranes were freeze-fractured in liquid nitrogen and then sputter-coated (Hitachi® E1020) with gold. The cross

section morphology of membranes was observed by a field-emitting scanning electron microscope (SEM) (Hitachi S-4800, Japan).

Energy dispersive X-ray spectrometry (EDS) measurement was used to analyze the element of the membrane using SEM (Hitachi S-4800, Japan) equipped with an Energy Dissipative X-ray Spectroscopic (GENESIS 60S).

Differential scanning calorimetry (DSC) (Perkin Elmer DSC-7) was used to measure the crystallinity ( $X_c$ ) of the membranes. The heating rate was 10 °C min<sup>-1</sup> and the temperature range was from 40 °C to 220 °C. The crystallinity was calculated based on the following equation from the DSC curves [27]:

$$X_c(\%) = \frac{\Delta H}{\Delta H_m \phi} \times 100 \quad (1)$$

Where,  $\Delta H$  and  $\Delta H_m$  represent the fusion enthalpy of the membrane and 100% crystalline PVDF, respectively. The value of  $\Delta H_m$  is 104.7 J g<sup>-1</sup> [27].  $\phi$  is the PVDF weight fraction in blend membrane.

Porosity of the membrane was measured according to the method reported by Wu et al. [18]. The membrane was immersed into n-butanol for 1 h and weighted before and after absorption the n-butanol. The porosity was calculated using the following equation:

$$P\% = \frac{\frac{M_b}{\rho_b}}{\left(\frac{M_p}{\rho_p}\right) + \left(\frac{M_b}{\rho_b}\right)} \times 100 \quad (2)$$

Where  $P\%$  is the porosity of membrane,  $M_p$  is the mass of membrane,  $M_b$  is the mass of absorbed n-butanol,  $\rho_p$  and  $\rho_b$  are the density of membrane and the n-butanol, respectively.

The mechanical properties of the membranes were measured using an Instron testing machine (AG-1 pull equipment, Japan). The tensile rate was 25 mm min<sup>-1</sup>. The measurement temperature was 25 °C. The size of the samples was 5.0 × 1.0 cm<sup>2</sup>. Each sample specimen was tested 5 times and even value was used to measure stress–strain curve.

## 2.6. Electrolyte solution uptake and leakage of polymer electrolytes

The dried porous polymer membrane was cut into a disk with a diameter of 2.4 cm. After the thickness and mass ( $W_0$ ) of the membrane disk was measured, it was soaked in electrolyte solution for 4 h at room temperature in the glove box, 4 h is long enough for fully infiltrating to activate the polymer electrolyte [28]. After the excrecent solution at the surface of the polymer electrolyte was absorbed with a piece of filter paper, the membrane was weighed ( $W_i$ ). The polymer electrolyte was weighed every 2 min at room temperature until to the constant weight, the weight ( $W_f$ ) and thickness recorded. In this study, the electrolyte uptake and leakage were tested according to Ma. [23] and calculated by the following equations:

$$\text{Electrolyte uptake} = \frac{W_f - W_0}{W_0} \times 100 \quad (3)$$

$$\text{Electrolyte leakage} = \frac{W_i - W_f}{W_i - W_0} \times 100 \quad (4)$$

Where  $W_0$  is the weight of dry membrane,  $W_i$  and  $W_f$  are the initial and equilibrium weight of the wet membrane after absorbing the liquid electrolyte, respectively.

Table 1

Code and composition of membranes and corresponding polymer electrolytes.

Blend membrane code	Composition PSF/PVDF (wt/wt)	Polymer electrolyte code	Blend membrane code	Composition PSF/PVDF (wt/wt)	Polymer electrolyte code
M0	0/100	E0	M3	6/100	E3
M1	2/100	E1	M4	8/100	E4
M2	4/100	E2	M5	10/100	E5

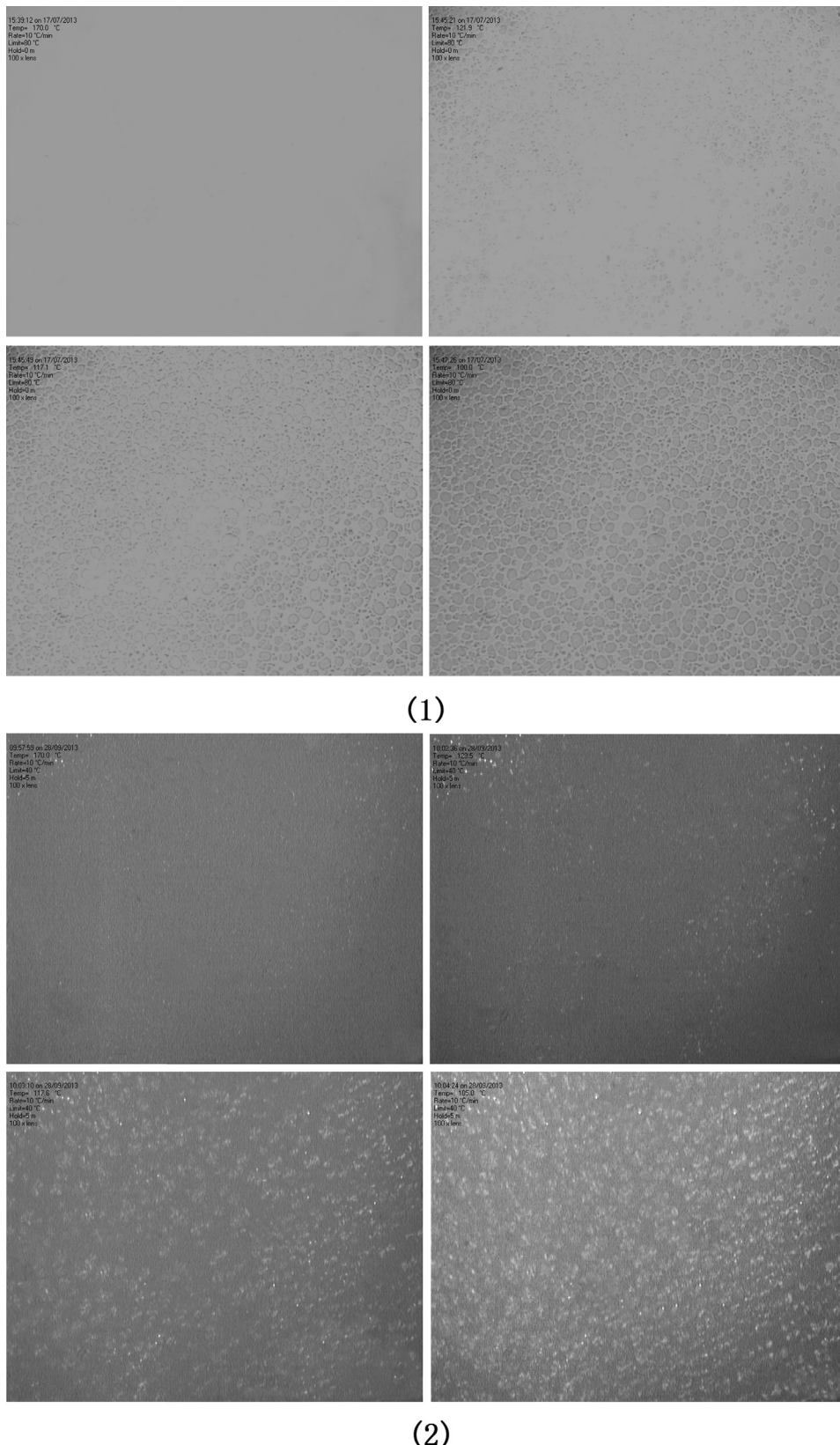


**Fig. 1.** Microphotographs for the systems at different cooling temperature (1) PSF/PVDF = 0/100, (2) PSF/PVDF = 2/100.

## 2.7. Electrochemical measurements

Coin cells (CR2430 size) were assembled in a glove box under dry argon (less than 2 mg L<sup>-1</sup> H<sub>2</sub>O). The electrochemical impedance spectroscopy was measured by electrochemical workstation (Zennium, German Zahner). The frequency range was from 1.0 MHz to 0.1 Hz. The measuring temperature range was from 0 °C to 80 °C. Each sample was measured 3 times.

The ionic conductivity ( $\sigma$ ) was calculated using the following equation [29]:

$$\sigma = \frac{1}{R_b} \frac{L}{A} \quad (5)$$

Where  $L$ ,  $A$  and  $R_b$  are thickness (cm), effective area (cm<sup>2</sup>) and bulk resistance (ohm) of polymer electrolyte, respectively.  $R_b$  was obtained from the high frequency of AC impedance intercept on the real axis. The effective area was 3.14 cm<sup>2</sup> and the thickness was in the range of 95–135 μm.

The electrochemical stability window was examined in a cell of Li foil/polymer electrolyte/SS by linear sweep voltammetry (LSV) at 5 mV s<sup>-1</sup>.

A mixture composed of 80 wt% LiFePO<sub>4</sub> powder, 10 wt% acetylene black and 10 wt% PVDF were mixed with NMP. The mixture was spread onto aluminum foil substrate and dried at 100 °C for 24 h in vacuum. After being cut to 1.3 cm × 1.3 cm size, the LiFePO<sub>4</sub> electrode was mounted as the positive electrode versus lithium tablet as the negative electrode in coin cell. The lithium/polymer electrolyte/LiFePO<sub>4</sub> cell was assembled in an argon-filled glove box. The cells were charged and discharged between 2.0 and 4.2 V at 25 °C on a battery tester (LAND CT2001A, Wuhan Land Electronic Co. Ltd.). The current density was 200 μA cm<sup>-2</sup> (0.5 C current rate). The 50 cycles were recorded.

## 3. Results and discussion

During the experiment, the following phenomena were observed.

Firstly, both PVDF and PSF could dissolve in DEDB as the temperature was higher than 180 °C. However, PVDF, PSF and DEDB could not form homogeneous system at 180 °C. Secondly, after DBP was added to the system in a suitable weight ratio (DEDB/DBP = 1/3 by weight), PVDF, PSF, DBP and DEDB could form homogeneous solution at 200 °C. Thirdly, phase separation between PVDF, PSF and diluent occurred at about 120 °C and 80 °C, respectively. Finally, DBP and DEDB were still miscible even the temperature decreased as low as 0 °C. These suggested that PVDF crystallization occurred before PSF solidification during the cooling process.

### 3.1. The phase diagram of the PVDF/PSF/diluent system

The phase diagram of a polymer/diluent system is usually composed of two lines: the binodal line drawn from  $T_{\text{cloud}}$  and the crystallization line drawn from  $T_c$ . L-L phase separation occurs within the region between the binodal line and the crystallization line. S-L phase separation occurs within the region under the crystallization line [11]. Fig. 1 presented the optical microscope images for the PVDF/PSF/diluent system at a decreased temperature. It can be seen that as the temperature decreased, no liquid droplets were observed. Instead, only the growth of spherulites could be observed. This suggested the occurrence of PVDF crystallization. According to Matsuyama et al. [30], if there exists L-L phase separation for a polymer/diluent system during the cooling process, the formation and growth of liquid droplets, which are composed of the polymer-lean phase, can be observed under the

optical microscope before the polymer begins to crystallize. If there exists only S-L phase separation for the polymer/diluent system, only the spherulites and their growth can be observed under the optical microscope during the cooling process. In this work, the appearance of only spherulites means that there is no cloud point and only the dynamic crystallization temperature for the PVDF/PSF/diluent system. In other words, only S-L phase separation occurs for the PVDF/PSF/diluent system during the cooling process. Therefore, as shown in Fig. 2, there exists only the crystallization line in phase diagram.

It can be seen from Fig. 2 that  $T_c$  increased with the increase of the PSF/PVDF weight ratio. This can be ascribed two features. One is the weakened interaction between PVDF and diluent. As mentioned above, PVDF crystallization occurred before PSF solidification during the cooling process. PSF and diluent can be regarded as one phase before PSF solidification. Thus, the addition of PSF weakened the interaction between PVDF and diluent due to the poor compatibility between PSF and PVDF. The more PSF was added, the weaker interaction between PVDF and diluent would be. The weak interaction promoted the accumulation and crystallization of PVDF molecules [31]. The other is the rigid segments of benzene ring in PSF molecules. The rigid segments can act as “nucleating agent” to promote the nucleation for PVDF crystallization. Therefore,  $T_c$  increased with the increase of PSF content.

### 3.2. Membrane morphology

Fig. 3 showed the cross-sections of SEM images from the membranes prepared with different PSF/PVDF weight ratio. It can be seen that spherulites, the typical structure formed via S-L phase separation process, were observed for all the membranes. This phenomenon is consistent with the results observed under the optical microscope in Fig. 1.

Further, with the increase of PSF/PVDF weight ratio, the size of spherulites decreased and the shape of spherulites became irregular. In the case of the system with only S-L phase separation, the change of membrane morphology can be ascribed to the interaction between polymer and diluent, the viscosity and the nucleation of benzene ring rigid segment in PSF molecules [11]. The system with high PSF/PVDF weight ratio presented weaker interaction between PVDF and diluent, higher viscosity and more rigid segments of benzene ring. Weaker interaction between PVDF and diluent and higher viscosity impeded the motion of PVDF segments. Thus, the

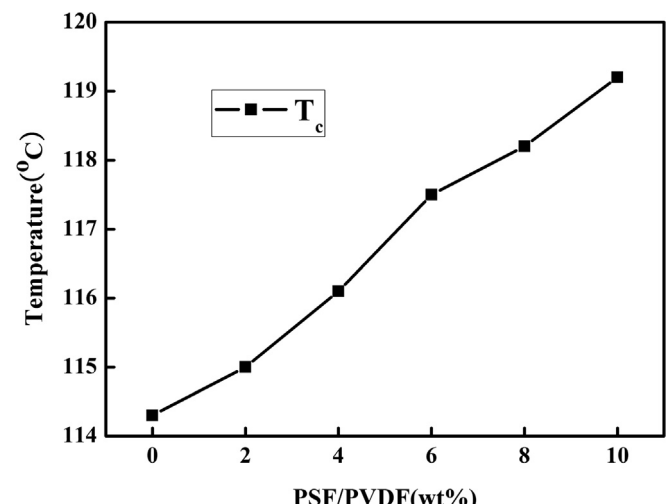
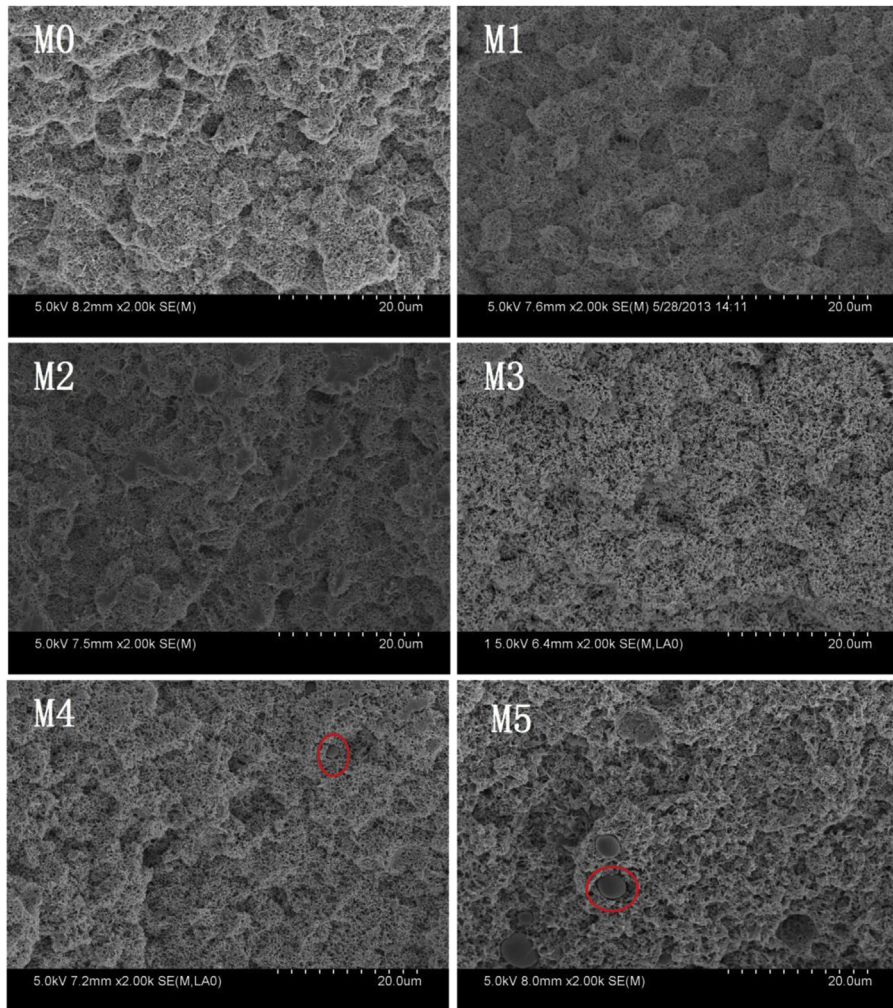


Fig. 2. Phase diagram of PVDF/PSF/diluent system.



**Fig. 3.** Cross-section SEM micrographs of membranes with different PSF/PVDF weight ratio.

shape of spherical particles became irregular. More rigid segments not only impeded the motion of PVDF segments but also promoted the nucleation of more primary nuclei at the beginning of PVDF crystallization. In the systems with the same PVDF concentration, more primary nuclei suggested less PVDF molecules to grow up. Therefore, the number of spherulite increased and the size of spherulite decreased.

It also can be seen from Fig. 2 that as the PSF/PVDF weight ratio was more than 8/100, some “spherical-shaped aggregates” (marked by rectangle), which were named as “big spherical crystalline particles” in this manuscript, could be found in the cross section of membrane. This suggested that macroscopic phase separation occurred between PVDF and PSF. This phenomenon was similar with the poly (vinyl chloride)/polyacrylonitrile/SiO<sub>2</sub> (PVC/PAN/SiO<sub>2</sub>) composite hollow fiber membrane reported by Mei et al. [32]. In order to verify the component of the “big spherical crystalline particles”, EDS measurement was employed. Fig. 3 illustrated the EDS analysis for M5. It can be seen from Fig. 4 1 and 2 that few “Sulfur” element in the matrix of membrane but a large amount of “sulfur” element was detected from “big spherical crystalline particles”. This demonstrated that the “big spherical crystalline particles” structures contained quite a high PSF.

The effect of PSF weight fraction on morphology of the membranes can be explained as follows. As the temperature decreased, PVDF would crystallize from the PVDF/PSF/diluent system but

amorphous PSF could not crystallize. PVDF formed primary nuclei at the beginning of polymer crystallization, and as the temperature further decreased, these primary nuclei grew out continuously to form lamellae and the aggregation of lamellae formed spherulites. PSF would be excluded from PVDF crystals during the process of PVDF crystallization. However, PSF might initially be mixed with PVDF in spite of its partial miscibility with PVDF. When the PSF/PVDF weight ratio was low (less than 8/100 in this manuscript), and the cooling rate was relatively fast in a 0 °C water bath, there was no enough time for PSF to be excluded by PVDF crystallization and a majority of PSF possibly resided between the PVDF crystalline lamellae, fibrils, spherulites, or some combinations of these. Only a small quantity of PSF was excluded and mixed with the amorphous domains and part crystal phase of PVDF, which located in the lamellae and spherulite surfaces. Therefore, what we observe in the SEM micrograph was spherulites. However, as the PSF/PVDF weight ratio was further increased (more than 8/100 in this manuscript), the amount of PSF that resided between crystalline lamellae, fibrils, spherulites, or some combinations of these, decreases. Therefore, more PSF was excluded and mixed with the amorphous domains and part crystal phase of PVDF. The higher the PSF/PVDF weight ratio was, the more excluded PSF would be. Moreover, it is impossible to thoroughly separate amorphous domains from crystal phase for PVDF during the crystallization. Therefore, PSF mixed with part of the PVDF crystal phase and the amorphous

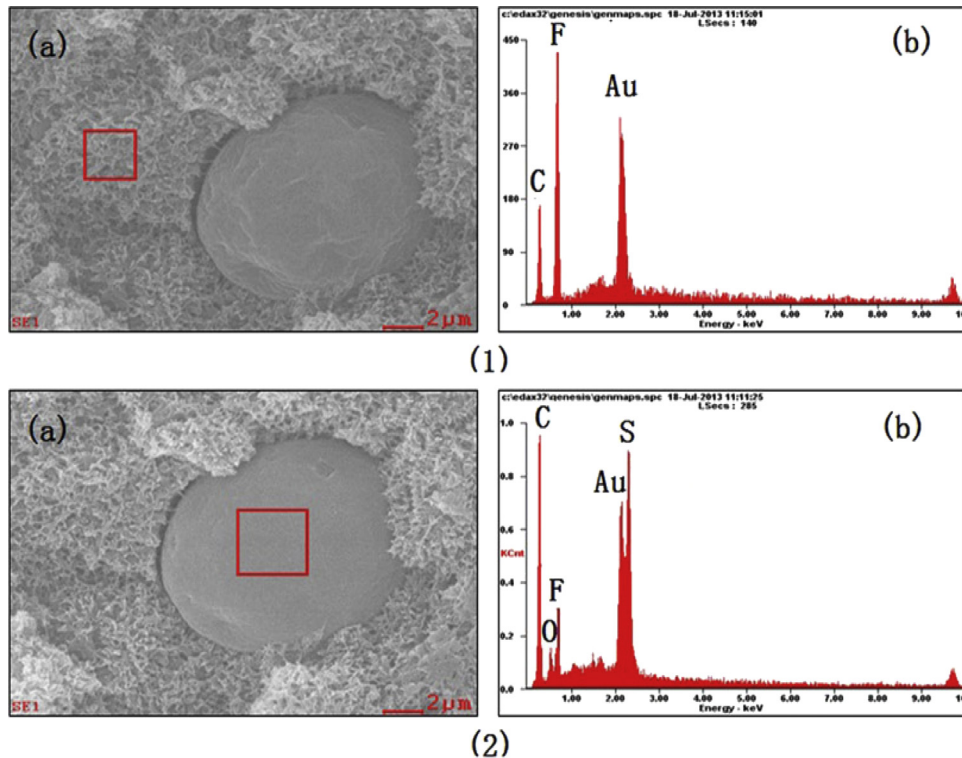


**Fig. 4.** EDS analysis of M5 (1) the membrane matrix, (2) the aggregate.

domains of PVDF and formed the “big spherical crystalline particles”.

Based on the results of phase diagram and SEM micrographs, the schematic diagram of phase separation process for the PVDF/PSF/diluent system was proposed in Fig. 5.

### 3.3. DSC analyses of the membranes

The melting temperature and crystallinity of the membranes were studied by DSC measurement. As shown in Fig. 6, the endotherm peak decreased from 175 °C to 171.8 °C as PSF/PVDF weight

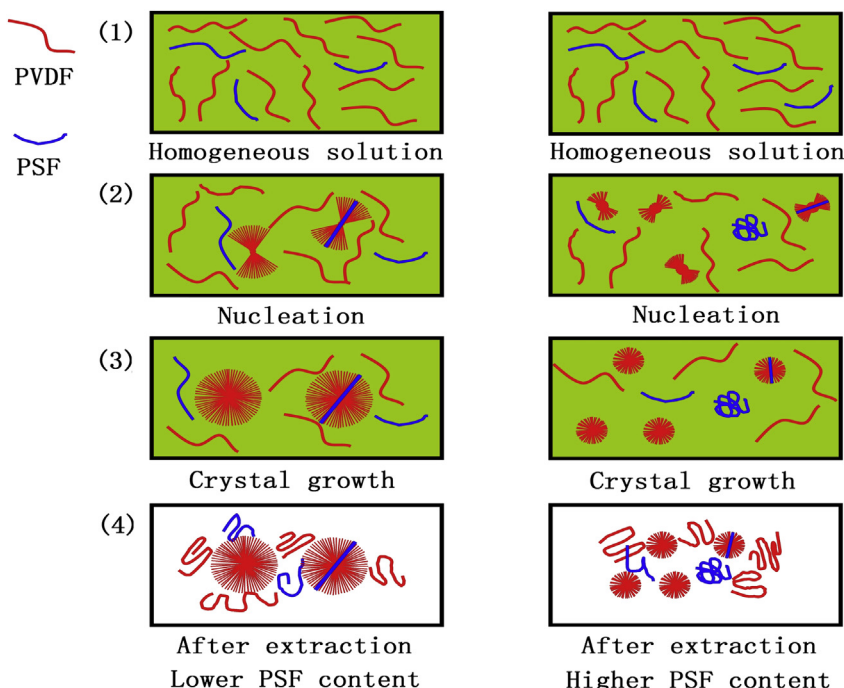


**Fig. 5.** Schematic diagram of phase separation process for the PVDF/PSF/diluent system.

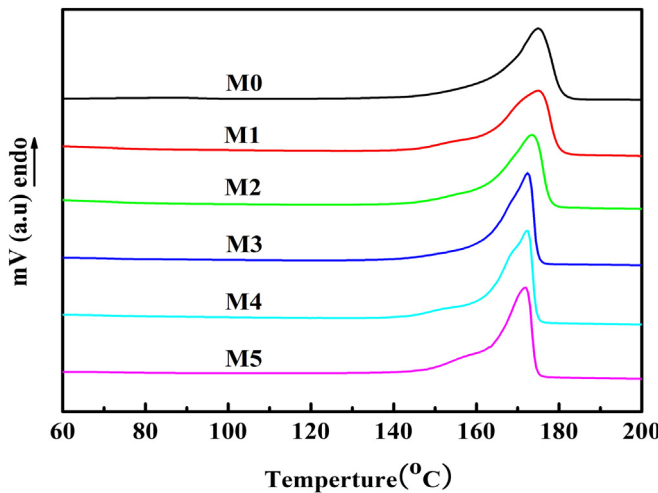


Fig. 6. DSC curves of membranes with different PSF/PVDF weight ratio.

ratio increased from 0/100 to 10/100. The shift of endotherm peaks can be explained by the Thompson–Gibbs equation [33]:

$$T_m = T_m^0 \left( 1 - \frac{2\sigma_e}{l\Delta h} \right) \quad (6)$$

Where,  $T_m$  and  $T_m^0$  represent the melting temperature and the equilibrium melting temperature of the membrane, respectively.  $\sigma_e$  is surface energy.  $l$  is the thickness of lamellae (i.e., the size of PVDF crystallite).  $\Delta h$  is the heat of fusion per unit volume of lamellae. It can be deducted from the equation that  $T_m$  is associated with  $l$ . The smaller the  $l$  is, the lower the  $T_m$  will be. For the PVDF/PSF system in this study, the size of spherulites decreased with the increase of PSF/PVDF weight ratio. Therefore,  $T_m$  decreased with the increase of PSF/PVDF weight ratio.

Table 2 listed the crystallinity of the membranes. It can be seen that the crystallinity decreased from 62.48% to 57.81% as the PSF/PVDF weight ratio increased from 0/100 to 6/100. However, the crystallinity increased from 57.81% to 68.41% as the PSF/PVDF weight ratio increased from 6/100 to 10/100. The change of crystallinity can be explained by the crystallization rate of PVDF/PSF/diluent system. The crystallization rate included the nucleation rate and growth rate. The increase of PSF/PVDF weight ratio, for one thing, increased the nucleation rate due to the nucleating function of PSF, on the other hand, increased the viscosity of PVDF/PSF/diluent system and hindered the growth rate. As the PSF/PVDF weight ratio was no more than 6/100, the increase of nucleation rate was less than the decrease of growth rate. Therefore, the crystallization rate, or the crystallinity, decreased. As the weight ratio of PSF/PVDF was more than 6/100, the nucleation rate further increased. However, the impediment of PSF on growth rate decreased due to the macroscopic phase separation between PSF and PVDF. Therefore, the crystallization rate, or the crystallinity, increased.

Table 2  
Crystallinity and porosity of membranes.

Code	$\Delta H$ (J g <sup>-1</sup> )	$X_c$ (%)	$\rho$ (%)	Code	$\Delta H$ (J g <sup>-1</sup> )	$X_c$ (%)	$\rho$ (%)
M0	65.42	62.48	54.98	M3	57.10	57.81	60.71
M1	63.63	61.99	57.95	M4	64.48	66.51	59.53
M2	60.98	60.57	58.36	M5	65.11	68.41	58.48

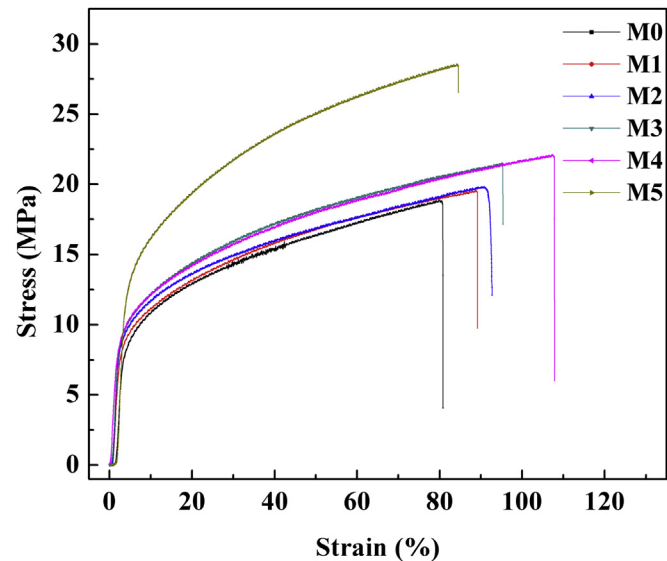


Fig. 7. Stress–strain curves of membranes with different PSF/PVDF weight ratio.

### 3.4. Porosity of the membranes

The pore of membrane provided a reservoir for liquid electrolyte in lithium ion batteries. Higher porosity led to higher electrolyte uptake and thus higher ionic conductivity of the corresponding polymer electrolyte. Table 2 listed the porosity of the blend membranes. It was found that the porosity of the blend membranes increased from 54.98% to 60.71% as the PSF/PVDF weight ratio increased from 0/100 to 6/100. This may be ascribed to the increased PSF content, which led to more amorphous domains for blend membranes. The more the amorphous domain was, the more diluent the membrane absorbed. Thus, more absorbed diluent led to more pores [34]. However, as the PSF/PVDF weight ratio increased from 6/100 to 10/100, the porosity of the blend membranes decreased slightly. This may be caused by the reduced amorphous domain of PVDF. The reduced amorphous domain led to less absorbed diluent and resulted in less pores formed in the subsequent extraction process.

### 3.5. Mechanical properties of the membranes

Fig. 7 described the stress–strain results of the membranes. Specific values of the mechanical properties were listed in Table 3. It can be seen that the break strength of the membrane increased from 18.67 MPa to 28.43 MPa as the PSF/PVDF weight ratio increased from 0 to 10/100. This suggested higher toughness of blend membranes. The elongation at break of membrane roughly increased to 107.78% as the PSF/PVDF weight ratio increased to 8/100 and then decreased to 84.57% as the PSF/PVDF weight ratio further increased to 10/100. The increase of the break strength and elongation at break can mainly ascribe to two aspects. One is the increase of PSF content, the other is the decrease of spherulite size. Rigid benzene ring in PSF increased toughness of membrane and

Table 3  
The values of stress and strain of membranes prepared with different PSF/PVDF weight ratio.

Code	M0	M1	M2	M3	M4	M5
Stress (MPa)	18.67	19.43	19.82	21.32	21.96	28.43
Strain (%)	80.68	88.23	91.91	94.98	107.78	84.53

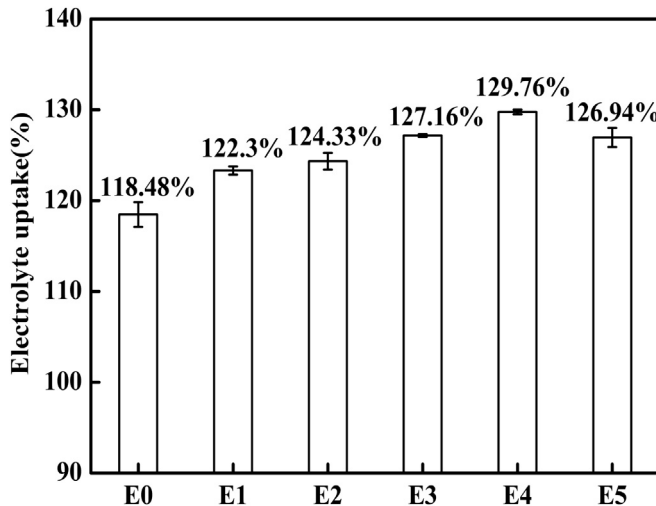


Fig. 8. Electrolyte uptakes of polymer electrolytes.

small spherulite size increased contact area between spherulites. The decrease of the elongation at break for M5 may be caused by the local macroscopic phase separation between PSF and PVDF.

### 3.6. Electrolyte uptake and electrolyte leakage of the polymer electrolytes

Fig. 8 displayed the electrolyte uptake of polymer electrolyte. It can be seen that as the PSF/PVDF weight ratio was less than 8/100, the electrolyte uptake of polymer electrolyte increased with the increase of PSF/PVDF weight ratio. However, as the PSF/PVDF weight ratio was more than 8/100, the electrolyte uptake of polymer electrolyte decreased with the increase of PSF/PVDF weight ratio. The maximum electrolyte uptake was 129.76% as the PSF/PVDF weight ratio was 8/100. The increase of electrolyte uptake in this manuscript can mainly be ascribed to the increase of porosity, the more swelled amorphous domain (the increased amount of the amorphous section of PVDF) and the more functional group having a good affinity with liquid electrolyte (the increased amount of PSF). For example, as PSF/PVDF weight ratio was in the range of 6/100–8/100, although porosity and amorphous domains of PVDF decreased slightly, the increased PSF suggested more functional

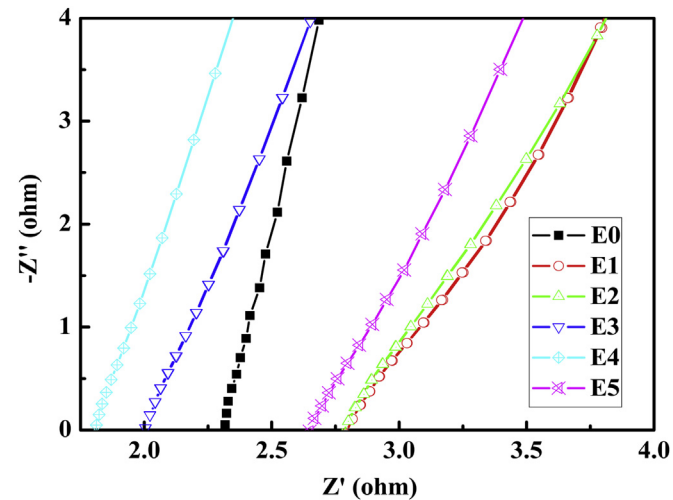


Fig. 10. The AC impedance plots of polymer electrolytes.

group to combine electrolyte solution, and thus increased electrolyte uptake.

Fig. 9 exhibited the relationship between the content of PSF and the electrolyte leakage of polymer electrolyte. It was found that the electrolyte leakage decreased from 44.74% to 37.35% as PSF/PVDF weight ratio increased from 0/100 to 6/100, and then increased slightly as PSF/PVDF weight ratio increased from 6/100 to 10/100. According to the research of Shi et al. [35], electrolyte leakage included two processes. That is, the liquid electrolyte transferred from the interior of polymer electrolyte to the surface layer, and the liquid electrolyte in the surface layer exuded through surface pores of polymer electrolyte. Therefore, electrolyte leakage was influenced by both the structure of interior and surface layer. In other words, the affinity between PSF and electrolyte, the swelled amorphous domain formed by PVDF amorphous domain and pore structure influenced electrolyte leakage. As PSF/PVDF weight ratio was less than 6/100, as shown in Fig. 3, the pore structure of blend membranes was similar. Therefore, the electrolyte leakage decreased with the increase of the swelled amorphous domain formed by PVDF amorphous domain and the content of PSF. As the PSF/PVDF weight ratio was more than 8/100, the increase of electrolyte leakage can be mainly ascribed to the decrease of the swelled amorphous domain formed by PVDF.

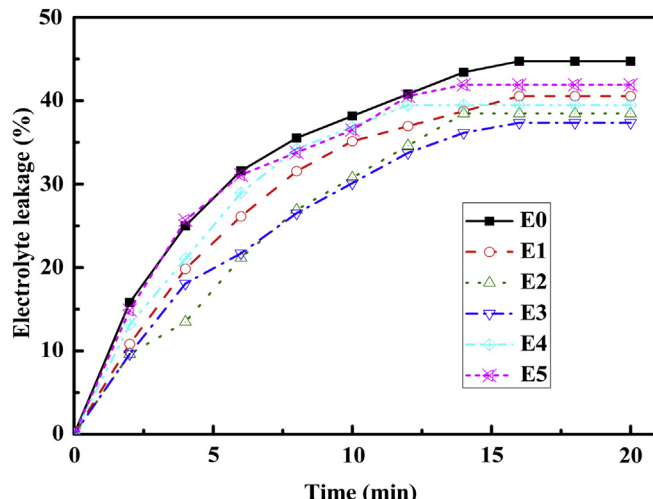


Fig. 9. Electrolyte leakages of polymer electrolytes.

### 3.7. Electrochemical properties of polymer electrolytes

The AC impedance spectra of polymer electrolytes were shown in Fig. 10. The values of bulk resistance ( $R_b$ ) were obtained from the high frequency intercept on the real axis.  $R_b$ , the thickness ( $L$ ) and the calculated values of ionic conductivity of polymer electrolytes at 20 °C were listed in Table 4. It can be found that the ionic conductivity increased from  $1.31 \times 10^{-3} \text{ S cm}^{-1}$  to the maximum  $2.03 \times 10^{-3} \text{ S cm}^{-1}$  as PSF/PVDF weight ratio increased from 0/100 to 8/100 and then decreased to  $1.55 \times 10^{-3} \text{ S cm}^{-1}$  as PSF/PVDF

**Table 4**  
Bulk resistance, thickness and ionic conductivity of polymer electrolytes.

Code	$R_b$ (ohm)	$L$ ( $\mu\text{m}$ )	$\sigma \times 10^{-3}$ ( $\text{S cm}^{-1}$ )	Code	$R_b$ (ohm)	$L$ ( $\mu\text{m}$ )	$\sigma \times 10^{-3}$ ( $\text{S cm}^{-1}$ )
E0	2.32	95	1.31	E3	2.01	120	1.91
E1	2.79	120	1.37	E4	2.12	135	2.03
E2	2.78	120	1.38	E5	2.26	110	1.55

weight ratio further increased to 10/100. The ionic conductivity was more than  $1.0 \times 10^{-3} \text{ S cm}^{-1}$ . As mentioned above, this value is the standard to determine whether the polymer electrolyte has a practical application [18].

Generally, ion conductivity is governed by the content and the mobility of carrier ions. It has been proved that the mechanism for the ionic conduction in the polymer electrolyte included two conduction paths. The two conduction paths consist of the swelled polymer phase (i.e., gel phase) and the pores full of liquid electrolyte [11]. In order to investigate which was the main conduction path, the cross-section structure of polymer electrolyte was employed. As shown in Fig. 11, compared with the membrane, the

cross-section structure of corresponding polymer electrolyte became denser with an increase in the amount of PSF. This suggested the decrease of porosity. This is because the amorphous domains of PVDF were easily swelled by liquid electrolyte to form gel phase. It also can be seen from Fig. 10 that there still exhibited some pores in all the samples. This meant that both the swelled polymer phase and pores full of liquid electrolyte were the conducting channel. In other words, the ionic conductivity was the combined effect of two conduction paths.

The temperature dependence of the ionic conductivity for the polymer electrolyte in the range of 0 °C–80 °C was presented in Fig. 12. It can be found that ionic conductivity increased with the

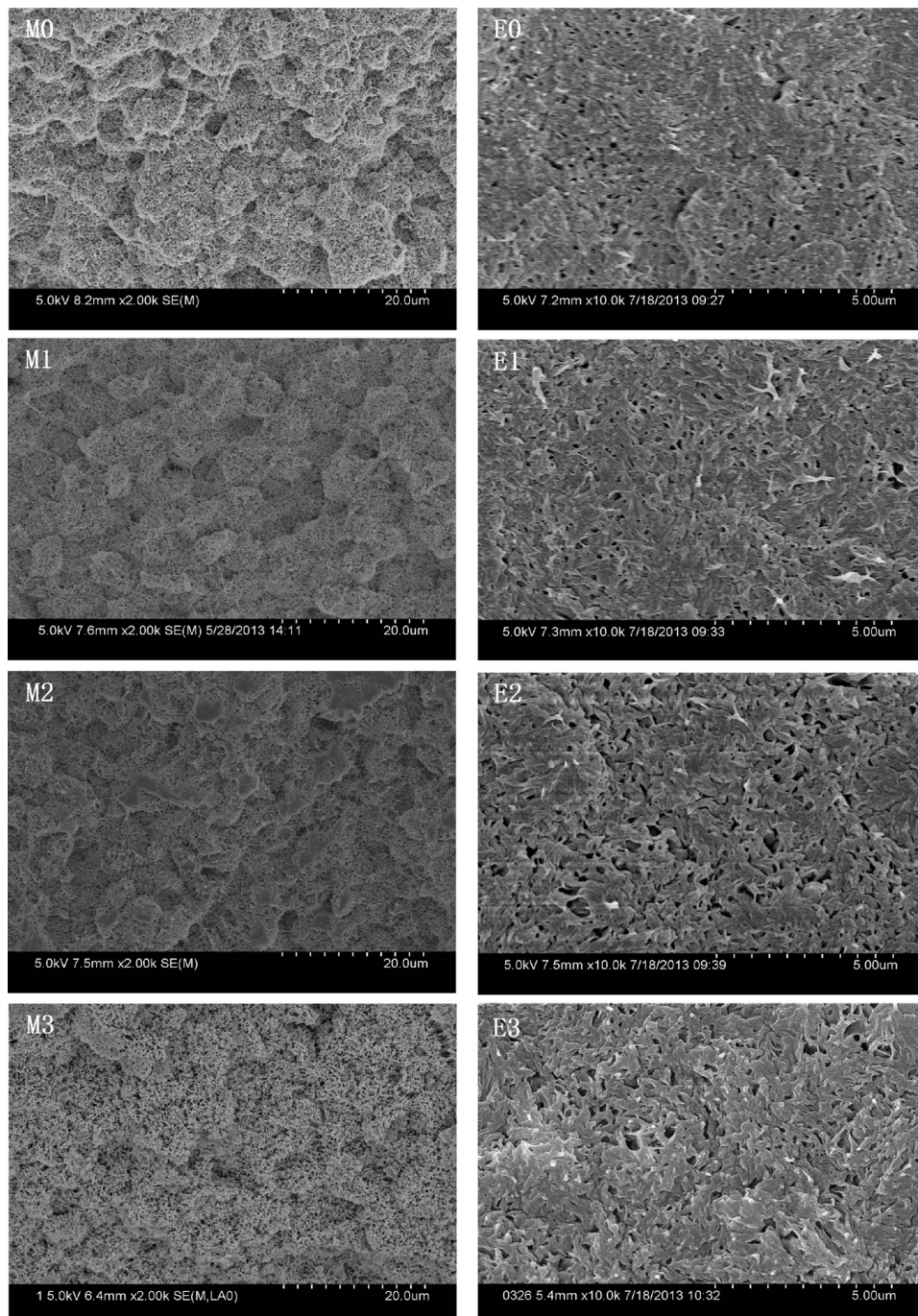


**Fig. 11.** Cross-section SEM micrographs of membranes and corresponding polymer electrolytes.

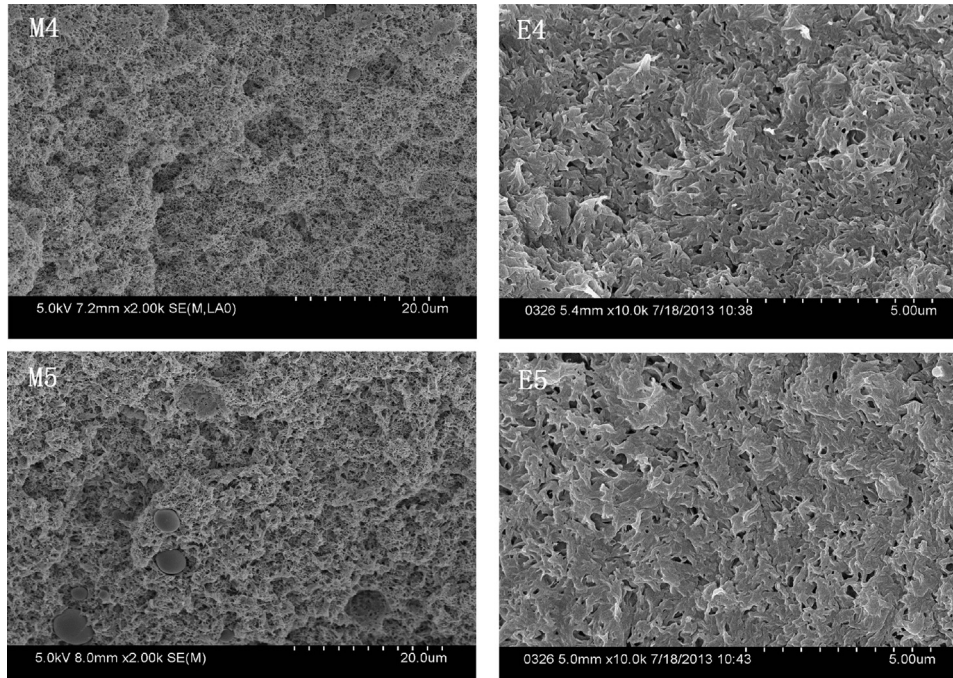


Fig. 11. (continued).

increase of temperature. This was the typical behavior for a polymer electrolyte. This is because a higher temperature not only promoted the migration of carrier ions but also resulted in the expansion of polymer. This expansion produced local empty space and increased the free volume, which promoted the motion of polymer segments and carrier ions. Moreover, the conductivity–temperature plot of all the membranes showed a curve relation. It further indicated that the swelled amorphous domains played an important role in the transfer of carrier ions [36].

The electrochemical stability of polymer electrolyte system should be electrochemically stable up at least 4.5 V (vs. Li<sup>+</sup>/Li) because sometimes the work potential reached to as high as 4.5 V for the practical lithium ion battery. The electrochemical stability window could be measured by the decomposition potential. As shown in Fig. 13, the decomposition potential increased from 4.6 V

to 4.9 V (vs. Li<sup>+</sup>/Li) as the PSF/PVDF weight ratio increased from 0/100 to 10/100. That is, the decomposition potential increased slightly with the increase of PSF/PVDF weight ratio. This phenomenon, which was different from the result of PVDF/PEO-PPO-PEO blend membranes [22] and PVDF/PMMA blend membranes [23], suggested that PSF increased the electrochemical stability of polymer electrolyte. No further explanations about the increase of decomposition potential were given in documents. The reason may be that the bond energy of S=O (522 kJ mol<sup>-1</sup>) for PSF was stronger than that of C–F (485 kJ mol<sup>-1</sup>) for PVDF, which in turn suggested that PSF was more difficult to decompose than PVDF. However, further study is necessary to verify the explanation. The values of decomposition potential showed that the blend PVDF/PSF polymer electrolytes prepared in this study were suitable for application in lithium ion batteries.

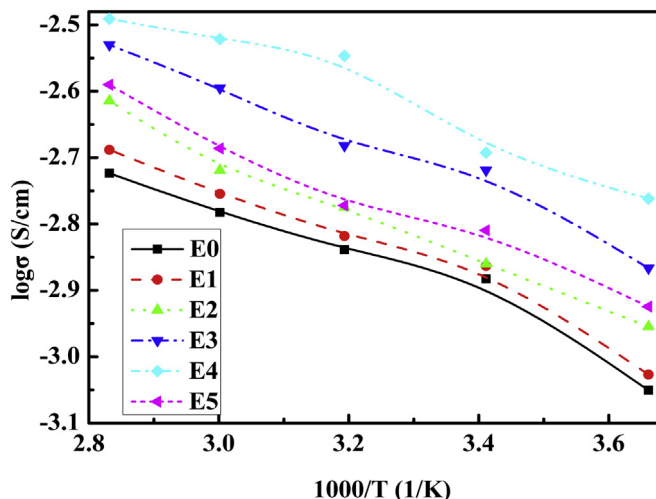


Fig. 12. Temperature dependence of the ionic conductivity for polymer electrolytes.

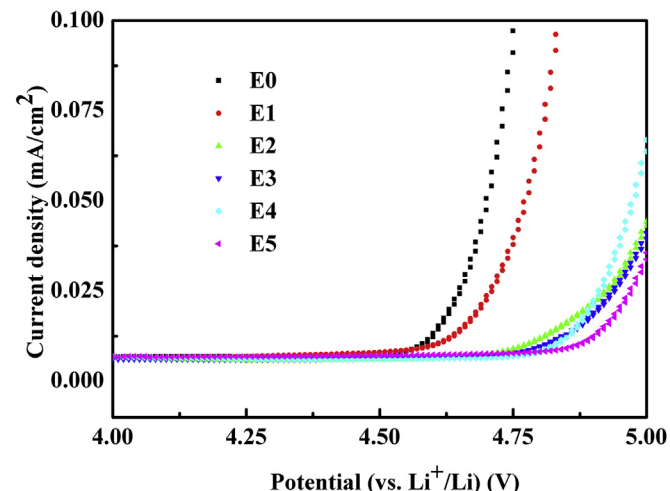


Fig. 13. Electrochemical stability windows of SS/polymer electrolyte/Li cells.

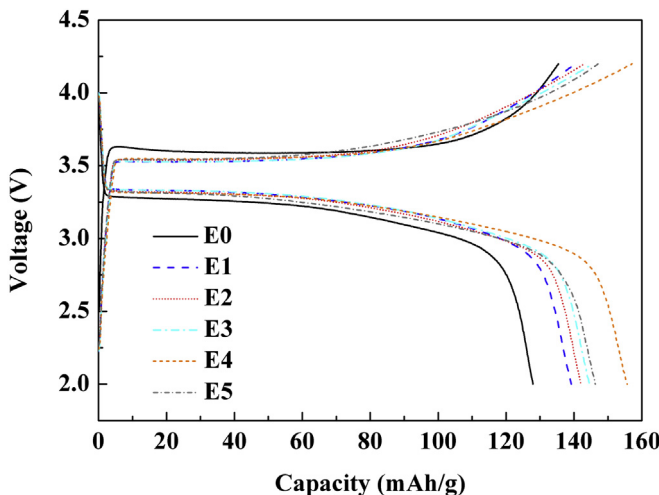


Fig. 14. Initial charge–discharge capacities of lithium/polymer electrolyte/LiFePO<sub>4</sub> cells with different PSF/PVDF weight ratio at 200  $\mu\text{A cm}^{-2}$  current density.

Fig. 14 showed the initial charge–discharge curve of the lithium/polymer electrolyte/LiFePO<sub>4</sub> cells using polymer electrolytes with different PSF/PVDF weight ratio at 200  $\mu\text{A cm}^{-2}$  current density. A flat plateau between 3.3 V and 3.7 V can be seen from all charge–discharge curves. This was a typical characteristic of LiFePO<sub>4</sub> [37]. The positive electrode operated on the following reversible process.



The theoretical specific capacity of LiFePO<sub>4</sub> was 170 mAh g<sup>-1</sup> [38]. The initial charge and discharge capacity of the cells increased from 135.40 mAh g<sup>-1</sup> and 133.19 mAh g<sup>-1</sup> to 157.22 mAh g<sup>-1</sup> and 155.69 mAh g<sup>-1</sup> as PSF/PVDF weight ratio increased from 0/100 to 8/100, then decreased to 147.11 mAh g<sup>-1</sup> and 146.30 mAh g<sup>-1</sup> as the PSF/PVDF weight ratio further increased to 10/100. The lithium/E4/LiFePO<sub>4</sub> showed the maximum capacity for all samples. This may be ascribed to the higher ionic conductivity because higher ionic conductivity facilitated the repeated intercalation/deintercalation of carrier ions in/from the electrode materials [39]. According to the initial charge and discharge capacity, the coulombic efficiency of

the initial cycle can be calculated. It can be found that the initial coulombic efficiency of blend polymer electrolyte was higher than that of the polymer electrolyte without blending. It has been well known that the coulombic efficiency of initial cycle is closely related the irreversible capacity, which arises from the reductive decomposition of electrolyte solution at the first cycle. The increase of initial coulombic efficiency revealed that PSF can reduce the reductive decomposition of electrolyte solution to some extent.

The cycling stability of the lithium/electrolyte/LiFePO<sub>4</sub> cells with different PSF/PVDF weight ratio was evaluated by measuring the discharge capacity of cells at 200  $\mu\text{A cm}^{-2}$  current density. It can be seen from Fig. 15 that the discharge capacity of the cells gradually decreased with an increase of the cycle. Compared with the polymer electrolytes without blending, the cells of blend polymer electrolytes showed higher discharge capacity and better capacity retention. The E4 showed higher capacity retention than other polymer electrolytes. The discharge capacity for the cell lithium/E4/LiFePO<sub>4</sub> was still as high as 145.31 mAh g<sup>-1</sup> after 50 cycles. This may be ascribed to that E4 can afford more facile ionic transport resulted from its higher electrolyte uptake [40].

#### 4. Conclusions

PVDF/PSF blend membranes were successfully prepared via TIPS technique. The phase diagram indicated that the PVDF/PSF/diluent system underwent S–L phase separation. The addition of PSF decreased the size of PVDF spherulite. This suggested that for TIPS process, it is possible to control membrane structure by blending the polymer which was poor compatible with the polymer matrix. The modest addition of PSF increased porosity, decreased crystallinity, enhanced electrolyte uptake of membranes and enhanced the ionic conductivity of corresponding polymer electrolyte. The further addition of PSF decreased the porosity of membrane and the performance of corresponding polymer electrolytes to some extent. The maximum electrolyte uptake of membrane was 129.76% and the maximum ionic conductivity of corresponding polymer electrolyte was  $2.03 \times 10^{-3}$  S cm<sup>-1</sup> at 20 °C. The addition of PSF increased the electrochemical stability window of polymer electrolyte. The electrochemical stability window of all samples was stable up to 4.5 V (vs. Li<sup>+</sup>/Li). Compared with the polymer electrolyte without blending, the lithium/polymer electrolyte/LiFePO<sub>4</sub> cell of blend polymer electrolyte showed higher charge–discharge capacity and better discharge performance at 200  $\mu\text{A cm}^{-2}$  current density. The investigations demonstrated that PVDF/PSF blend microporous membranes prepared via TIPS technique could be used as polymer matrices of polymer electrolytes for lithium ion batteries.

#### Acknowledgments

This work was finally supported by the National Nature Foundation of China (No. 51003074), China Postdoctoral Science Foundation (No. 2013M541183), the Program for Changjiang Scholars and Innovative Research Team in University (PCSIRT) of Ministry of Education of China (No. IRT13084) and Foundation of National Engineering Research Center for Compounding and Modification of Polymer Materials (No. FK201301).

#### References

- [1] J.M. Tarascon, M. Armand, *Nature* 414 (2001) 359–367.
- [2] A.S. Arico, P.G. Bruce, B. Scrosati, J.M. Tarascon, W.V. Schalkwijk, *Nat. Mater.* 4 (2005) 366–377.
- [3] Z. Jiang, B. Carroll, K.M. Abraham, *Electrochim. Acta* 42 (1997) 2667–2677.
- [4] P. Periasamy, K. Tatsumi, M. Shikano, T. Fujieda, T. Sakai, Y. Saito, M. Mizuhata, A. Kajinami, S. Deki, *Solid State Ionics* 126 (1999) 285–292.

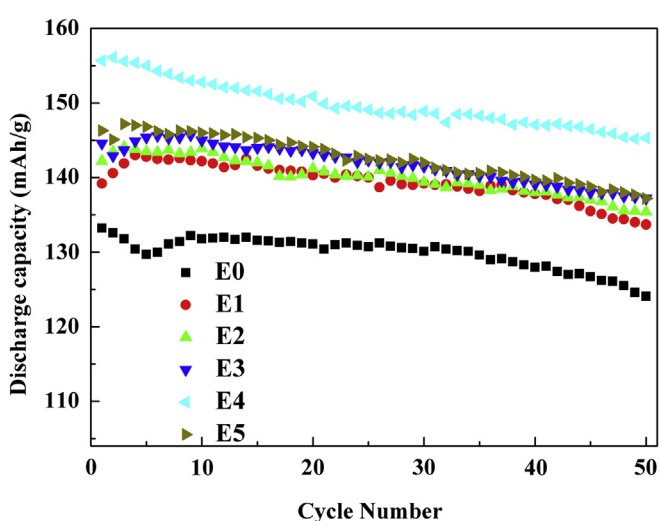


Fig. 15. Performances of lithium/polymer electrolyte/LiFePO<sub>4</sub> cells with different PSF/PVDF weight ratio at 200  $\mu\text{A cm}^{-2}$  current density.

[5] Q.W. Lu, J.H. Fang, J. Yang, R.R. Miao, J.l. Wang, Y. Nuli, *J. Membr. Sci.* 449 (2014) 176–183.

[6] A.S. Gozdz, C.N. Schmutz, J.M. Tarascon, P.C. Warren, U. S. Pat. 5540741, 1997.

[7] A. Magistris, P. Mustarelli, F. Parazzoli, E. Quartarone, P. Piaggio, A. Bottino, *J. Power Sources* 97–98 (2001) 657–660.

[8] G.L. Ji, B.K. Zhu, C.F. Zhang, Y.Y. Xu, *J. Appl. Polym. Sci.* 107 (4) (2008) 2109–2117.

[9] Y. Saito, H. Kataoka, E. Quartarone, P. Mustarelli, *J. Phys. Chem. B* 106 (2002) 7200–7208.

[10] S.D. Smith, G.H. Shipman, R.M. Floyd, H.T. Freemyer, S.J. Hamrock, M.A. Yandrasits, D.G.S. Walton, WO patent WO 2005/035641.

[11] G.L. Ji, B.K. Zhu, Z.Y. Cui, C.F. Zhang, Y.Y. Xu, *Polymer* 48 (2007) 6415–6425.

[12] S. Rajabzadeh, C. Ling, Y. Ohmukai, T. Maruyama, H. Matsuyama, *J. Membr. Sci.* 423–424 (2012) 189–194.

[13] Y.G. Li, Y. Su, C.X. Chen, *Membr. Sci. Technol.* 26 (4) (2006) 10–13.

[14] M.Y. Jeon, C.K. Kim, *J. Membr. Sci.* 300 (2007) 172–181.

[15] P.D. Radovanovic, M.A. Perez, S.D. Thomas, US Pat: 6461724 B1, 2002-10-8.

[16] S.S. Zhang, *J. Power Sources* 164 (2007) 351–364.

[17] A. Kumar, M. Deka, S. Banerjee, *Solid State Ionics* 181 (2010) 609–615.

[18] C.G. Wu, M.I. Lu, H.J. Chuang, *Polymer* 46 (2005) 5929–5938.

[19] R.R. Qiu, H. Matsuyama, H. Zhong, H.Q. Ye, K.L. Huang, *Sep. Sci. Eng. Chin. J. Chem. Eng.* 18 (2) (2010) 207–216.

[20] R. LV, J. Zhou, Q.G. Du, H.T. Wang, W. Zhong, *J. Membr. Sci.* 281 (2006) 700–706.

[21] C.F. Zhang, Y.X. Bai, Y.P. Sun, J. Gu, Y.Y. Xu, *J. Membr. Sci.* 365 (2010) 216–224.

[22] Z.Y. Cui, Y.Y. Xu, L.P. Zhu, J.Y. Wang, Z.Y. Xi, B.K. Zhu, *J. Membr. Sci.* 325 (2008) 957–963.

[23] T. Ma, Z.Y. Cui, Y. Wu, S.H. Qin, H. Wang, F. Yan, *J. Membr. Sci.* 444 (2013) 213–222.

[24] X.X. Ma, F.M. Shi, W.J. Zhao, M.N. Wu, J. Zhang, J. Ma, C.J. Gao, *Desalination* 303 (2012) 39–47.

[25] C.L. Song, Y.M. Cao, X.M. Jie, H.J. Yu, G.D. Kang, J.H. Liu, Q. Yuan, *Membr. Sci. Technol.* 30 (4) (2010) 14–18.

[26] Y.B. Yun, J.D. Li, R.Y. Ma, *Membr. Sci. Technol.* 25 (5) (2005) 10–14, 20.

[27] J.H. Cao, B.K. Zhu, Y.Y. Xu, *J. Membr. Sci.* 281 (2006) 446–453.

[28] Z.Y. Cui, Y.Y. Xu, L.P. Zhu, X.Z. Wei, C.F. Zhang, B.K. Zhu, *Mater. Lett.* 62 (2008) 3809–3811.

[29] C.L. Cheng, C.C. Wan, Y.Y. Wang, *J. Power Sources* 134 (2003) 202–210.

[30] H. Matsuyama, T. Maki, M. Teramoto, K. Asano, *J. Membr. Sci.* 204 (2002) 323–328.

[31] Y. Su, C.X. Chen, Y.G. Li, J.D. Li, *J. Macromol. Sci. Pure Appl. Chem.* 44 (2007) 305–313.

[32] S. Mei, C.F. Xiao, X.Y. Hu, W. Shu, *Desalination* 280 (2011) 378–383.

[33] R.G. Jin, Y.Q. Hua, *Polymer Physics*, third ed., Chemical Industry Press, Beijing, China, 2009, pp. 157–158.

[34] Z.Y. Cui, Y.Y. Xu, *J. Macromol. Sci. Part B* 49 (2010) 301–318.

[35] Q. Shi, M. Yu, X. Zhou, Y.S. Yan, C.R. Wan, *J. Power Sources* 103 (2001) 286–292.

[36] O. Bohnke, G. Frand, M. Rezrazi, C. Rousselot, C. Truche, *Solid State Ionics* 66 (1993) 97–104.

[37] N.H. Idris, M.M. Rahman, J.Z. Wang, H.K. Liu, *J. Power Sources* 201 (2012) 294–300.

[38] V. Gentili, S. Panero, P. Reale, B. Scrosati, *J. Power Sources* 170 (2007) 185–190.

[39] K. Hanai, M. Ueno, N. Imanishi, A. Hirano, O. Yamamoto, Y. Takeda, *J. Power Sources* 196 (2011) 6756–6761.

[40] H.S. Jeong, S.Y. Lee, *J. Power Sources* 196 (2011) 6716–6722.

## A list of symbols

$T_{cloud}$ : the cloud point

$T_c$ : the dynamic crystallization temperature

$T_m$ : the melting temperature

$X_c$ : the crystallinity

$\Delta H$ : the fusion enthalpy of the membrane

$\Delta H$ : the fusion enthalpy of PVDF with 100% crystallinity

$\varphi$ : the PVDF weight fraction in blend membrane

$P$ : the porosity of membrane

$M_p$ : the mass of membrane

$M_b$ : the mass of absorbed n-butanol

$\rho_p$ : the density of membrane

$\rho_b$ : the density of n-butanol

$W_o$ : the weight of dry membrane

$W_i$ : the initial weight of membrane after absorbing liquid electrolyte

$W_f$ : the equilibrium weight of membrane after absorbing liquid electrolyte

$\sigma$ : the ionic conductivity

$R_b$ : the bulk resistance of polymer electrolyte

$L$ : the thickness of polymer electrolyte

$A$ : the area of polymer electrolyte